Bull Math Biol (2014) 76:3051–3069
DOI 10.1007/s11538-014-0044-6

Society for Mathematical Biology

ORIGINAL ARTICLE

Stochastic Turing Patterns: Analysis of Compartment-Based Approaches

Yang Cao · Radek Erban

Received: 28 October 2013 / Accepted: 5 November 2014 / Published online: 25 November 2014

Abstract Turing patterns can be observed in reaction-diffusion systems where chemical species have different diffusion constants. In recent years, several studies investigated the effects of noise on Turing patterns and showed that the parameter regimes, for which stochastic Turing patterns are observed, can be larger than the parameter regimes predicted by deterministic models, which are written in terms of partial differential equations (PDEs) for species concentrations. A common stochastic reaction-diffusion approach is written in terms of compartment-based (lattice-based) models, where the domain of interest is divided into artificial compartments and the number of molecules in each compartment is simulated. In this paper, the dependence of stochastic Turing patterns on the compartment size is investigated. It has previously been shown (for relatively simpler systems) that a modeler should not choose compartment sizes which are too small or too large, and that the optimal compartment size depends on the diffusion constant. Taking these results into account, we propose and study a compartment-based model of Turing patterns where each chemical species is described using a different set of compartments. It is shown that the parameter regions where spatial patterns form are different from the regions obtained by classical deterministic PDE-based models, but they are also different from the results obtained for the stochastic reaction-diffusion models which use a single set of compartments for all chemical species. In particular, it is argued that some previously reported results on the effect of noise on Turing patterns in biological systems need to be reinterpreted.

Y. Cao
Department of Computer Science, Virginia Tech, Blacksburg, VA 24061, USA
e-mail: ycao@vt.edu

R. Erban (✉)
Mathematical Institute, University of Oxford, Radcliffe Observatory Quarter, Woodstock Road, Oxford OX2 6GG, UK
e-mail: erban@maths.ox.ac.uk

Keywords Stochastic Turing patterns · Compartment-based models · Stochastic reaction-diffusion systems · Multigrid discretization

1 Introduction

In his pioneering work, Turing (1952) showed that stable spatial patterns can develop in reaction-diffusion systems which include chemical species (morphogens) with different diffusion constants. Considering a system of two chemical species with concentrations $u(x,t)$ and $v(x,t)$ in a one-dimensional interval $x \in [0, L]$, the underlying deterministic model of Turing patterns can be written as a system of two reaction-diffusion partial differential equations (PDEs)

$$\frac{\partial u}{\partial t} = D_u \frac{\partial^2 u}{\partial x^2} + f_1(u, v), \tag{1}$$

$$\frac{\partial v}{\partial t} = D_v \frac{\partial^2 v}{\partial x^2} + f_2(u, v), \tag{2}$$

where D_u and D_v are diffusion constants of morphogens u and v, respectively, and $f_1(u, v)$ and $f_2(u, v)$ describe chemical reactions. Then, the standard analysis proceeds as follows (Murray 2002; Satnoianu et al. 2000): a homogeneous steady state $u(x,t) \equiv u_s$, $v(x,t) \equiv v_s$ is found by solving $f_1(u_s, v_s) = 0$ and $f_2(u_s, v_s) = 0$. It is shown that the homogenous steady state is stable when $D_u = D_v$, and conditions on f_1, f_2, D_u and D_v are obtained which guarantee that the homogeneous steady state will become unstable for $D_u \neq D_v$. Then, Turing patterns are observed at the steady state.

The above argument was extensively analyzed in the mathematical biology literature, and conditions for Turing patterns have been determined (Murray 2002; Satnoianu et al. 2000). Experimental studies with chemical systems (chlorite-iodide-malonic acid reaction) demonstrated Turing type patterns (Kepper et al. 1991; Quyang and Swinney 1991). There has also been experimental evidence that a simple Turing patterning mechanism can appear in developmental biology, for example, in the regulation of hair follicle patterning in developing murine skin (Sick et al. 2006). One of the criticisms of Turing patterns is their lack of robustness (Maini et al. 2012). The PDE system (1)–(2) can have several stable non-homogeneous solutions which the system can achieve with relatively small perturbations to the initial condition. Considering PDEs in a suitably growing domain, one can obtain an additional constraint on the system which restricts the set of accessible patterns, increasing the robustness of pattern generation with respect to the initial conditions (Crampin et al. 1999; Barrass et al. 2006). However, to assess the sensitivity of patterns with respect to fluctuations, stochastic models have to be considered (Maini et al. 2012; Black and McKane 2012).

One of the most common approaches to stochastic reaction-diffusion modeling is formulated in the compartment-based (lattice-based) framework (Erban et al. 2007). In the one-dimensional setting, the compartment-based analogue of the PDE model (1)–(2) can be formulated as follows: The computational domain $[0, L]$ is divided into K compartments of length $h = L/K$. We denote the number of molecules of chemical species U (resp. V) in the i-th compartment $((i-1)h, ih)$ by U_i (resp. V_i), $i = 1, 2, \ldots, K$. Then, the diffusion of U and V is described by the following chains of "chemical reactions" (Erban et al. 2007):

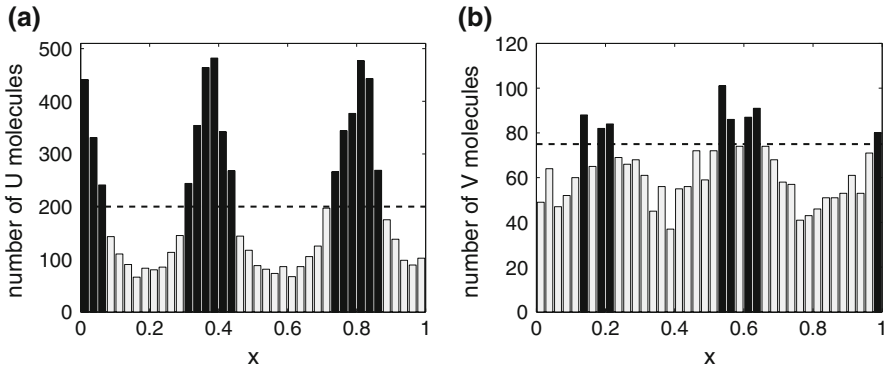

Fig. 1 Turing patterns for the stochastic reaction-diffusion system (3), (4) and (6). **a** Numbers of molecules of chemical species U in each compartment at time 18; **b** the same plot for chemical species V. The initial condition was the homogeneous steady state $U_{\text{st}} = 200$ and $V_{\text{st}} = 75$ for the parameters given in the text. The values of U_{st} and V_{st} are denoted by *dashed lines*. Adapted from Erban et al. (2007) with permission

$$U_1 \underset{d_u}{\overset{d_u}{\rightleftarrows}} U_2 \underset{d_u}{\overset{d_u}{\rightleftarrows}} U_3 \underset{d_u}{\overset{d_u}{\rightleftarrows}} \dots \underset{d_u}{\overset{d_u}{\rightleftarrows}} U_K, \tag{3}$$

$$V_1 \underset{d_v}{\overset{d_v}{\rightleftarrows}} V_2 \underset{d_v}{\overset{d_v}{\rightleftarrows}} V_3 \underset{d_v}{\overset{d_v}{\rightleftarrows}} \dots \underset{d_v}{\overset{d_v}{\rightleftarrows}} V_K \tag{4}$$

where

$$d_u = \frac{D_u}{h^2} \quad \text{and} \quad d_v = \frac{D_v}{h^2}. \tag{5}$$

Reactions are localized to each compartment. For example, considering the commonly studied Schnakenberg reaction system (Schnakenberg 1979), chemical reactions in the i-th compartment are described by (Qiao et al. 2006):

$$\emptyset \underset{k_2}{\overset{k_1}{\rightleftarrows}} U_i, \qquad \emptyset \xrightarrow{k_3} V_i, \qquad 2U_i + V_i \xrightarrow{k_4} 3U_i. \tag{6}$$

The above formulation (3), (4) and (6) describes the stochastic reaction-diffusion model as a system of $(8K - 4)$ chemical reactions: We have $(K - 1)$ diffusive jumps of U molecules to the left (resp. right), $(K - 1)$ diffusive jumps of V molecules to the left (resp. right) and $4K$ reactions (6). This system can be simulated using the Gillespie algorithm (Gillespie 1977), or its equivalent formulations (Cao et al. 2004; Gibson and Bruck 2000). In Fig. 1, we present an illustrative simulation of the reaction-diffusion system (3), (4) and (6). We clearly see that Turing patterns can be observed for the chosen set of dimensionless parameters: $k_1 = 4 \times 10^3$, $k_2 = 2$, $k_3 = 1.2 \times 10^3$, $k_4 = 6.25 \times 10^{-8}$, $D_u = 10^{-3}$ and $D_v = 10^{-1}$. Compartment values above (resp. below) the homogeneous steady-state values $U_{\text{st}} = 200$ and $V_{\text{st}} = 75$ are colored black (resp. light gray) to visualize stochastic Turing patterns. Let us note that the rate constants k_1 and k_3 are production rates per unit of area. The stochastic model uses the

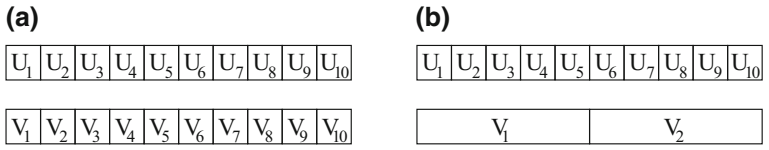

Fig. 2 **a** Schematic of the uniform discretization. **b** Schematic of different meshes used for U and V where γ defined by (12) is equal to 5

production rates per one compartment which are given as $k_1 h$ and $k_3 h$, respectively. More details of this stochastic simulation are given in Sect. 2 where we introduce the corresponding propensity functions (10)–(11).

The compartment-based approach has been used for both theoretical analysis and computational modeling (Scott et al. 2011; Hattne et al. 2005). The regions where stochastic Turing patterns can be expected were calculated using the linear noise analysis (Biancalani et al. 2010; McKane et al. 2014; Butler and Goldenfeld 2011). These studies were also generalized to growing domains (Woolley et al. 2011a, b), to stochastic reaction-diffusion models with delays (Woolley et al. 2012), to non-local trimolecular reactions (Biancalani et al. 2011) and to stochastic Turing patterns on a network (Asslani et al. 2012). Compartment-based software packages were developed (Hattne et al. 2005) and applied to modeling biological systems (Fange and Elf 2006). Computational approaches were also generalized to non-regular compartments (lattices) and complex geometries (Engblom et al. 2009; Isaacson and Peskin 2006). Stochastic simulations of Turing patterns (Twomey 2007; Fu et al. 2008; Hori and Hara 2012) and excitable media (Vigelius and Meyer 2012) were also presented in the literature. However, these theoretical and computational studies use the same discretization for each chemical species. In this paper, we will demonstrate that, in the case of Turing patterns, this simplifying assumption can undesirably bias the obtained theoretical and computational results.

One of the assumption of the compartment-based modeling is that compartments are small enough so that they can be assumed well-mixed. In particular, the relative size of diffusion and reaction constants determine the appropriate size of the compartment (Erban and Chapman 2009; Isaacson 2009; Hellander et al. 2012). It can be shown that there exists a limitation on the compartment size from below whenever the reaction-diffusion system includes a bimolecular reaction (Erban and Chapman 2009; Isaacson 2009; Hellander et al. 2012). There are also bounds on the compartment size from above (Kang et al. 2012; Hu et al. 2014), again the diffusion constant plays an important role in these estimates. In the case of Turing patterns, we have chemical species with different diffusion constants. For example, in the illustrative simulation in Fig. 1, we have $D_v/D_u = 100$, i.e., the diffusion constant of V is 100-times larger than the diffusion constant of U. However, we used the same discretization for both U and V which is schematically denoted in Fig. 2a. If we take into account that V diffuses much faster, then one could also consider the discretization in Fig. 2b where one compartment in the V variable corresponds to several compartments in the U variable. In this paper, we will study differences between discretizations in Fig. 2a, b. We will show that these discretizations lead to different parameter regimes for stochastic Turing patterns.

The paper is organized as follows. In Sect. 2, we introduce and analyze a simple test problem which will be used to illustrate our results. It will be based on the above model (3), (4) and (6). In Sect. 3, we analyze both types of discretizations, considering a simple two-compartment discretization in U. Illustrative numerical results are presented in Sect. 4. We conclude this paper with the discussion of our results in Sect. 5.

2 Deterministic and Stochastic Models of an Illustrative Reaction-Diffusion System

We will consider a simple one-dimensional Schnakenberg model (6) where the reaction rate constants are given by (Qiao et al. 2006)

$$k_1 = \omega, \qquad k_2 = 2, \qquad k_3 = 3\omega, \qquad k_4 = \frac{1}{\omega^2} \tag{7}$$

and ω is a scale factor. We used $\omega = 4 \times 10^3$ in the illustrative simulation in Fig. 1. When there is no diffusion involved, the dynamics of this system can be represented as the system of reaction rate ordinary differential equations (ODEs)

$$\begin{aligned} \frac{\mathrm{d}u}{\mathrm{d}t} &= k_1 - k_2 u + k_4 u^2 v, \\ \frac{\mathrm{d}v}{\mathrm{d}t} &= k_3 - k_4 u^2 v, \end{aligned}$$

which has a unique stable steady state at $u_\mathrm{s} = 2\omega$ and $v_\mathrm{s} = 3\omega/4$. When we consider diffusion, the reaction-diffusion PDEs (1)–(2) are given by

$$\frac{\partial u}{\partial t} = D_u \frac{\partial^2 u}{\partial x^2} + k_1 - k_2 u + k_4 u^2 v, \tag{8}$$

$$\frac{\partial v}{\partial t} = D_v \frac{\partial^2 v}{\partial x^2} + k_3 - k_4 u^2 v. \tag{9}$$

We are implicitly assuming homogeneous Neumann boundary conditions (zero-flux) in the whole paper, but both the PDE model (8)–(9) and its stochastic counterparts could also be generalized to different types of boundary conditions (Erban and Chapman 2007). Using standard analysis of Turing instabilities (Qiao et al. 2006; Murray 2002), one can show that the Turing patterns are obtained for $D_v > 39.6 D_u$ for the parameter values (7). This condition is independent of ω. The illustrative simulation in Fig. 1 was computed for $D_v/D_u = 100$, i.e., the condition for (deterministic, mean-field) Turing patterns was satisfied.

When we are concerned with the stochastic effects, the reaction-diffusion system can be simulated by the Gillespie stochastic simulation algorithm with the one-dimensional computational domain $[0, L]$ discretized. Considering uniform discretization in Fig. 2a, the stochastic model is given as a set of "chemical reactions" (3), (4) and (6). Denoting the compartment length by h, we have the following propensity functions in the i-th compartment (Gillespie 1977; Qiao et al. 2006):

$$\alpha_1 = k_1 h, \quad \alpha_2 = k_2 U_i, \quad \alpha_3 = k_3 h, \quad \alpha_4 = \frac{k_4}{h^2} U_i (U_i - 1) V_i, \tag{10}$$

$$\alpha_5 = \alpha_6 = d_u U_i, \quad \alpha_7 = \alpha_8 = d_v V_i, \tag{11}$$

where d_u and d_v are given by (5). The first four propensities (10) are for the four chemical reactions in (6). The propensities (11) are for the diffusive jumps (left and right) for U (indices 5 and 6) and V (indices 7 and 8) which correspond to (3) and (4), respectively. In the illustrative simulation in Fig. 1, we divided interval $[0, 1]$ into $K = 40$ compartments, i.e., $h = 1/40 = 0.025$. In particular, the production rate of U molecules in one compartment was equal to $\alpha_1 = k_1 h = \omega h = 100$. The homogeneous steady state in compartments corresponded to values $U_{\text{st}} = u_s h = 2\omega h = 200$ and $V_{\text{st}} = v_s h = 3h\omega/4 = 75$.

2.1 Formulation of the Generalized Compartment-Based Model

The compartmentalization in Fig. 2b generalizes (3) and (4) to the case where different discretizations are used for U and V. We will denote by K_u (resp. K_v) the number of compartments in the U (resp. V) variable. We define the compartment lengths by

$$h_u = \frac{L}{K_u}, \qquad h_v = \frac{L}{K_v}, \qquad \text{and} \qquad \gamma = \frac{K_u}{K_v} = \frac{h_v}{h_u}, \tag{12}$$

where γ is the ratio of compartment sizes in the V and U variable. In what follows, we will consider that γ is an integer. For example, the schematic diagram in Fig. 2b used $\gamma = 5$. Then, the diffusion model is formulated as follows

$$U_1 \underset{d_u}{\overset{d_u}{\rightleftarrows}} U_2 \underset{d_u}{\overset{d_u}{\rightleftarrows}} U_3 \underset{d_u}{\overset{d_u}{\rightleftarrows}} \dots \underset{d_u}{\overset{d_u}{\rightleftarrows}} U_{K_u}, \tag{13}$$

$$V_1 \underset{d_v}{\overset{d_v}{\rightleftarrows}} V_2 \underset{d_v}{\overset{d_v}{\rightleftarrows}} V_3 \underset{d_v}{\overset{d_v}{\rightleftarrows}} \dots \underset{d_v}{\overset{d_v}{\rightleftarrows}} V_{K_v}, \tag{14}$$

where

$$d_u = \frac{D_u}{h_u^2}, \qquad d_v = \frac{D_v}{h_v^2} = \frac{D_v}{D_u \gamma^2} d_u. \tag{15}$$

In the standard compartment-based model (3) and (4), we have $\gamma = 1$. One option to choose γ in the generalized model (13) and (14) is to ensure that $d_u = d_v$ which implies

$$\gamma = \sqrt{\frac{D_v}{D_u}}. \tag{16}$$

Then, the jump rates d_u and d_v from the corresponding compartments are equal for molecules of U and V. However, we will not restrict to the case (16) and consider general choices of γ in this paper. The generalization of the first three propensities in (10) is straightforward. Propensities α_1 and α_2 in (10) correspond to chemical species

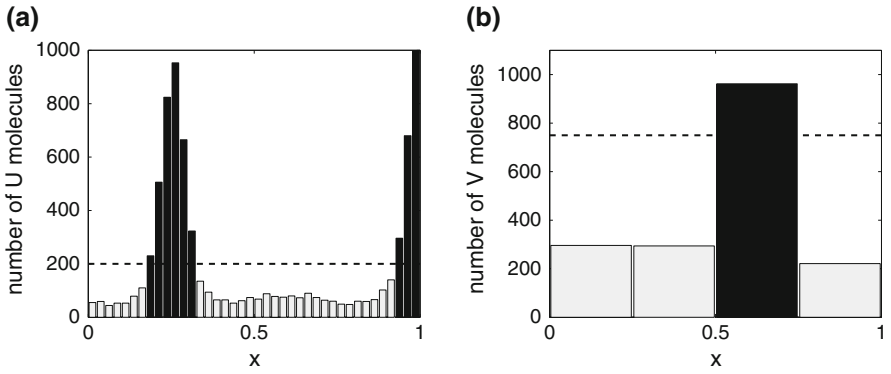

Fig. 3 Turing patterns computed by the generalized compartment-based model (13)–(17). **a** Numbers of molecules of chemical species U in each compartment at time 18; **b** the same plot for chemical species V. The initial condition was the homogeneous steady state $U_{\mathrm{st}} = 200$ and $V_{\mathrm{st}} = 750$ for the parameters given in the text. The values of U_{st} and V_{st} are denoted by *dashed lines*

U, and we have the following propensities in the i-th compartment, $i = 1, 2, \ldots, K_u$: $\alpha_1 = k_1 h_u$ and $\alpha_2 = k_2 U_i$. The propensity α_3 in (10) is considered in the j-th compartment corresponding to the V species, i.e., in the compartment $\big((j-1)h_v, jh_v\big)$. It is given as $\alpha_3 = k_3 h_v$. To generalize α_4, we have to consider the occurrences of the trimolecular reaction

$$2U + V \xrightarrow{k_4} 3U$$

in every small compartment used for the discretization of the U variable. In the i-th compartment, the propensity function α_4 is:

$$\alpha_4 = \frac{k_4}{h_u^2} U_i (U_i - 1) \frac{V_j}{\gamma}, \tag{17}$$

where V_j corresponds to the j-th compartment in the V variable to which the i-th compartment belongs, i.e.,

$$\big((i-1)h_u, ih_u\big) \subset \big((j-1)h_v, jh_v\big).$$

The main idea of the compartment-based model is that the molecules of V are considered to be well-mixed in the compartments of the size h_v. Thus, the propensity function (17) correctly generalizes the propensity of trimolecular reaction α_4 in the smaller compartment of length h_u.

In Fig. 3, we present an illustrative simulation of the generalized compartment-based model (13)–(17). We use the same parameters as in Fig. 1 to enable direct comparisons, i.e., k_1, k_2, k_3, k_4 are given by (7) where the scale factor $\omega = 4 \times 10^3$. We use (16) to select the value of γ. Since $D_u = 10^{-3}$ and $D_v = 10^{-1}$, the formula (16) implies $\gamma = 10$. We use the same number of compartments for U variable as in Fig. 1: $K_u = 40$. Using $\gamma = 10$, we obtain that V is discretized into $K_v = 4$ compartments. In Fig. 3, we see that the Turing pattern can still be clearly observed. As in

Fig. 1, compartment values above (resp. below) the homogeneous steady-state values $U_{\text{st}} = 200$ and $V_{\text{st}} = 75\gamma = 750$ are colored black (resp. light gray) to visualize stochastic Turing patterns.

Since the compartments for the V variable are 10-times larger in Fig. 3b than in Fig. 1b, it is not surprising that the numbers of molecules of V (per compartment) increased by the factor of 10. However, we can also notice that the numbers of molecules of U per compartment quantitatively differ in Figs. 1a and 3a (black peaks are twice as tall). An open question is to quantify these differences. In this paper, we show that even qualitative differences can be observed in some parameter regimes, where the generalized compartment-based model exhibits Turing patterns, while the original model does not.

The generalized compartment-based model (13) and (14) can be used to construct computational approaches to speed-up simulations of the standard compartment-based model, because it does not simulate all diffusion events for chemical species with large diffusion constants (Li and Cao 2012, 2014). For example, the illustrative simulation in Fig. 3 simulates ten times less compartments for V and is less computationally intensive than the original simulation in Fig. 1. However, in this work, we are interested in a different question than discussing numerical errors with different discretization strategies. We will investigate the Turing pattern formation under different discretizations. We will argue that the classical compartment-based approach is not the best starting point to analyze noise in systems which have chemical species with different diffusion constants. This conclusion can be already demonstrated if we consider a simple two-compartment model as we will see in the next section.

3 Analysis of Compartment-Based Models for $K_u = 2$

We will consider that the domain $[0, L]$ is divided into two compartments in the U variable, i.e., $K_u = 2$. Then, we have two possible options for the discretization of the quickly diffusing chemical species V:

(i) $\gamma = 1$ which corresponds to the classical compartment-based model where $K_v = 2$;
(ii) $\gamma = 2$ which corresponds to the generalized compartment-based model where $K_v = 1$.

We will start with the latter case which includes three variables U_1, U_2 and V_1 and is easier to analyze. In Sect. 3.2, we compare our results with the classical compartment-based approach.

3.1 Generalized Compartment-Based Model: $K_u = 2$ and $K_v = 1$

We consider the case where the whole interval $[0, L]$ is divided into two compartments for U and one compartment for V. The discretization is illustrated in Fig. 4a. We will denote by u_1, u_2 and v_1 the average numbers of molecules of U_1, U_2 and V_1 as predicted by the corresponding mean-field model. They satisfy the following system of three ODEs (Erban et al. 2007)

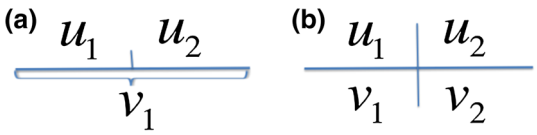

Fig. 4 **a** Generalized compartment-based model for $K_u = 2$ and $K_v = 1$: The interval is divided into two compartments for U and remains as one compartment for V. **b** Classical compartment-based model: The interval is divided into two compartments for both U and V

$$\frac{\mathrm{d}u_1}{\mathrm{d}t} = d_u(u_2 - u_1) + k_1 h_u - k_2 u_1 + \frac{k_4}{h_u h_v} u_1^2 v_1, \tag{18}$$

$$\frac{\mathrm{d}u_2}{\mathrm{d}t} = d_u(u_1 - u_2) + k_1 h_u - k_2 u_2 + \frac{k_4}{h_u h_v} u_2^2 v_1, \tag{19}$$

$$\frac{\mathrm{d}v_1}{\mathrm{d}t} = k_3 h_v - \frac{k_4}{h_u h_v}\left(u_1^2 + u_2^2\right) v_1. \tag{20}$$

We will study the stability of its steady states. In order to find the steady state, we let the left-hand side terms be zero. The corresponding algebraic equations can be written in the following form:

$$d_u(u_2 - u_1) + \frac{k_1 L}{2} - k_2 u_1 + \frac{2k_4}{L^2} u_1^2 v_1 = 0, \tag{21}$$

$$d_u(u_1 - u_2) + \frac{k_1 L}{2} - k_2 u_2 + \frac{2k_4}{L^2} u_2^2 v_1 = 0, \tag{22}$$

$$k_3 L - \frac{2k_4}{L^2}(u_1^2 + u_2^2) v_1 = 0, \tag{23}$$

where we used $h_u = L/K_u = L/2$ and $h_v = L/K_v = L$. Adding all three equations, we have

$$u_1 + u_2 = \frac{(k_1 + k_3)L}{k_2} = 2\omega L, \tag{24}$$

where we used the parameter choice (7). Let $u_1 = (1 + r)\omega L$ and $u_2 = (1 - r)\omega L$. Solving (23) for v_1, we obtain

$$v_1 = \frac{k_3 L^3}{2k_4(u_1^2 + u_2^2)} = \frac{3\omega L}{4(1 + r^2)}. \tag{25}$$

Substituting (25) back to (21), we have

$$-2d_u\, r\, \omega L + \frac{k_1 L}{2} - k_2(1 + r)\omega L + 2k_4(1 + r)^2\omega^2 \frac{3\omega L}{4(1 + r^2)} = 0.$$

Using the parameter choice (7), we can simplify it to

$$r\left[(1 - 2d_u) - 2(1 + d_u)r^2\right] = 0. \tag{26}$$

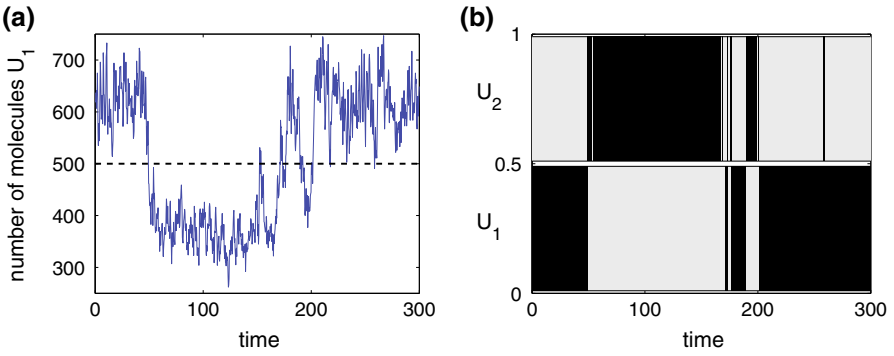

Fig. 5 **a** The time evolution of U_1 computed for the generalized compartment-based model with $K_u = 2$ and $K_v = 1$. The homogeneous steady state $u_s^2 = 500$ is plotted using the *dashed line*. **b** The time-dependent pattern given by the values of U_1 and U_2 computed for the same realization of the Gillespie algorithm as in the panel (*a*)

The system will have a non-homogeneous solution $u_1 \neq u_2$ if and only if the equation (26) has a nonzero solution, and that requires $2d_u < 1$. Using (15) and $h_u = L/2$, we obtain

$$D_u < \frac{L^2}{8}. \tag{27}$$

If this condition is satisfied, then the system has two non-nonhomogeneous steady-state solutions

$$u_1 = (1 \pm r)\omega L, \qquad u_2 = (1 \mp r)\omega L, \qquad v_1 = \frac{3\omega L}{4(1+r^2)}, \tag{28}$$

where

$$r = \sqrt{\frac{L^2 - 8D_u}{2L^2 + 8D_u}}. \tag{29}$$

In Fig. 5, we illustrate this result. We use $L = 1$, $D_u = 0.1$ and $\omega = 500$. Then, $r = 0.27$ and the steady-state values of u_1 (resp. u_2 are):

$$u_s^1 \doteq 366, \qquad u_s^2 \doteq 500, \qquad u_s^3 \doteq 634.$$

In Fig. 5a, we present the time evolution of U_1 computed by the Gillespie algorithm. We initialize the system at the steady state $[U_1(0), U_2(0), V_1(0)] = [634, 366, 350]$. We clearly see that the system is capable of switching between this state and the second non-homogeneous state. In Fig. 5b, we visualize the corresponding time-dependent pattern. As in Figs. 1 and 3, we plot the values which are larger than the homogeneous steady state $u_s^2 = 500$ in black. Light gray color denotes the values which are lower than $u_s^2 = 500$. We plot both U_1 and U_2 values in Fig. 5b to visualize the resulting pattern.

3.2 Classical Compartment-Based Model: $K_u = 2$ and $K_v = 2$

Next, we consider the case where the whole interval $[0,\ L]$ is divided into two compartments for both U and V. The discretization is illustrated in Fig. 4b. Denoting u_1, u_2, v_1 and v_2 the average numbers of molecules obtained by the corresponding mean-field model, they satisfy the following system of four ODEs (Erban et al. 2007)

$$\begin{aligned}
\frac{\mathrm{d}u_1}{\mathrm{d}t} &= d_u(u_2 - u_1) + k_1 h_u - k_2 u_1 + \frac{k_4}{h_u h_v} u_1^2 v_1,\\
\frac{\mathrm{d}u_2}{\mathrm{d}t} &= d_u(u_1 - u_2) + k_1 h_u - k_2 u_2 + \frac{k_4}{h_u h_v} u_2^2 v_2,\\
\frac{\mathrm{d}v_1}{\mathrm{d}t} &= d_v(v_2 - v_1) + k_3 h_v - \frac{k_4}{h_u^2} u_1^2 v_1,\\
\frac{\mathrm{d}v_2}{\mathrm{d}t} &= d_v(v_1 - v_2) + k_3 h_v - \frac{k_4}{h_u^2} u_2^2 v_2.
\end{aligned}$$

Again letting the left-hand side terms be zero and using $h_u = h_v = L/2$, we obtain the following system of algebraic equations

$$2d_u(u_2 - u_1) + k_1 L - 2k_2 u_1 + \frac{8k_4}{L^2} u_1^2 v_1 = 0, \tag{30}$$

$$2d_u(u_1 - u_2) + k_1 L - 2k_2 u_2 + \frac{8k_4}{L^2} u_2^2 v_2 = 0, \tag{31}$$

$$2d_v(v_2 - v_1) + k_3 L - \frac{8k_4}{L^2} u_1^2 v_1 = 0, \tag{32}$$

$$2d_v(v_1 - v_2) + k_3 L - \frac{8k_4}{L^2} u_2^2 v_2 = 0. \tag{33}$$

Adding all equations together, we have

$$u_1 + u_2 = \frac{(k_1 + k_3)L}{k_2} = 2\omega L. \tag{34}$$

Adding (32) and (33), we also have

$$u_1^2 v_1 + u_2^2 v_2 = \frac{k_3 L^3}{4k_4} = \frac{3\omega^3 L^3}{4}. \tag{35}$$

Adding (30) and (32), we obtain

$$(k_1 + k_3)L - 2k_2 u_1 + 2d_u(u_2 - u_1) + 2d_v(v_2 - v_1) = 0. \tag{36}$$

Using (34), we have $u_1 = (1 + r)\omega L$ and $u_2 = (1 - r)\omega L$ for a suitable r. Thus, (36) can be rewritten as

$$v_2 - v_1 = \frac{2r(1 + d_u)\omega L}{d_v} = 2r R \omega L, \tag{37}$$

where we denoted $R = (1 + d_u)/d_v$. Substituting (37) into (32) and denoting $S = 1 + d_u = d_v R$, we have

$$v_1 = \frac{(3 + 4Sr)\omega L}{8(1 + r)^2}. \tag{38}$$

Similarly from (33), we have

$$v_2 = \frac{(3 - 4Sr)L\omega}{8(1 - r)^2}. \tag{39}$$

Substituting both (38) and (39) to (37), we obtain

$$\frac{3 - 4Sr}{8(1 - r)^2} - \frac{3 + 4Sr}{8(1 + r)^2} = 2Rr.$$

which can be simplified to the equation

$$r\left(4R\left(1 - r^2\right)^2 + 2S\left(1 + r^2\right) - 3\right) = 0.$$

We are looking for the non-homogeneous solution where $r \neq 0$. Denoting $y = r^2 > 0$, we have a quadratic equation

$$4Ry^2 + (2S - 8R)y + (4R + 2S - 3) = 0. \tag{40}$$

We will look for conditions such that the equation (40) has a solution $0 < y < 1$ (since $-1 < r < 1$). Let

$$f(y) = 4Ry^2 + (2S - 8R)y + (4R + 2S - 3). \tag{41}$$

Then, we have $f(1) = 4S - 3 = 1 + 4d_u > 0$. One can verify that if $f(0) > 0$, it is impossible for the equation $f(y) = 0$ to have a solution between 0 and 1. On the other hand, if $f(0) < 0$, we will definitely have a solution between 0 and 1. Thus, we have a necessary and sufficient condition

$$f(0) = 4R + 2S - 3 < 0, \tag{42}$$

which corresponds to the condition for d_u and d_v:

$$\frac{4}{d_v} + 2 < \frac{3}{1 + d_u}.$$

We note that $d_u = D_u/h^2$ and $d_v = D_v/h^2$, where $h = h_u = h_v = L/2$. Thus, the necessary and sufficient condition for patterns becomes

$$\frac{L^2}{D_v} + 2 < \frac{3L^2}{L^2 + 4D_u}. \tag{43}$$

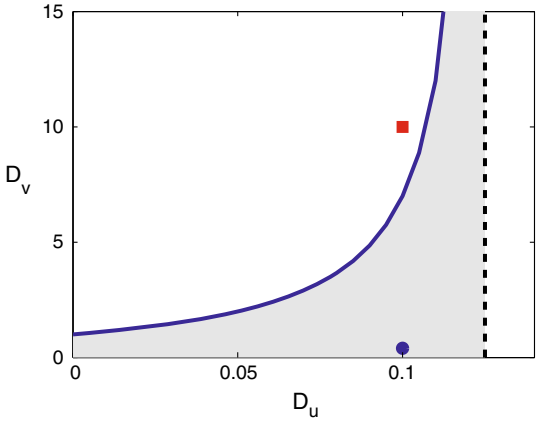

Fig. 6 The regions of patterning in D_u-D_v plane. The shaded area is the region where the standard compartment-based model does not yield patterns and the generalized compartment-based model has patterns. The (*blue*) circle is the parameter regime used in Fig. 7a, and the (*red*) square is the parameter regime used in Fig. 7b (Color figure online)

If $D_v \to \infty$, then the condition (43) becomes the condition (27) which was derived for the case of the generalized compartment-based model. The condition (27) is a necessary condition for (43) but not sufficient. We illustrate it in Fig. 6 for $L = 1$. The condition (27) corresponds to all parameter values to the left of the dashed line in Fig. 6. The condition (43) corresponds to the values of D_u and D_v which are above the (blue) solid line. The shaded area corresponds to parameter values for which the generalized compartment-based model yields non-homogeneous patterns and the standard compartment-based model does not. Next, we will use the same value of D_u as in Fig. 5, namely $D_u = 0.1$. We choose two values of D_v which are denoted as the (blue) circle and (red) square in Fig. 6. We use the Gillespie algorithm to simulate the standard compartment-based model for $K_u = K_v = 2$. The results are shown in Fig. 7. The top panels show the time evolution of U_1 and U_2. We clearly see the switching between two patterns for $D_v = 10$, but there is no bistability for $D_v = 0.4$. The resulting patterns are visualized in the bottom panels. As in Figs. 1, 3 and 5, we plot the values which are larger than the homogeneous steady state $u_s^2 = 500$ in black. Light gray color denotes the values which are lower than $u_s^2 = 500$.

Let us note that we are comparing the generalized compartment-based model with $K_u = 2$ and $K_v = 1$ with the classical compartment-based model. In particular, the generalized compartment-based model uses $\gamma = 2$. If we substitute $\gamma = 2$ in formula (16), we obtain $D_v = 4D_u$. In particular, the parameter values $D_u = 0.1$ and $D_v = 0.4$. are compatible with the choice (16). However, the standard compartment-based model does not exhibit patterns for this parameter choice as we observed in Fig. 7a.

Remark Let $z = L^2$. Then, the inequality (43) becomes

$$z^2 + (4D_u - D_v)z + 8D_u D_v < 0, \tag{44}$$

which is possible for some values of L if and only if

$$4D_u < D_v \quad \text{and} \quad (4D_u - D_v)^2 - 32D_u D_v > 0. \tag{45}$$

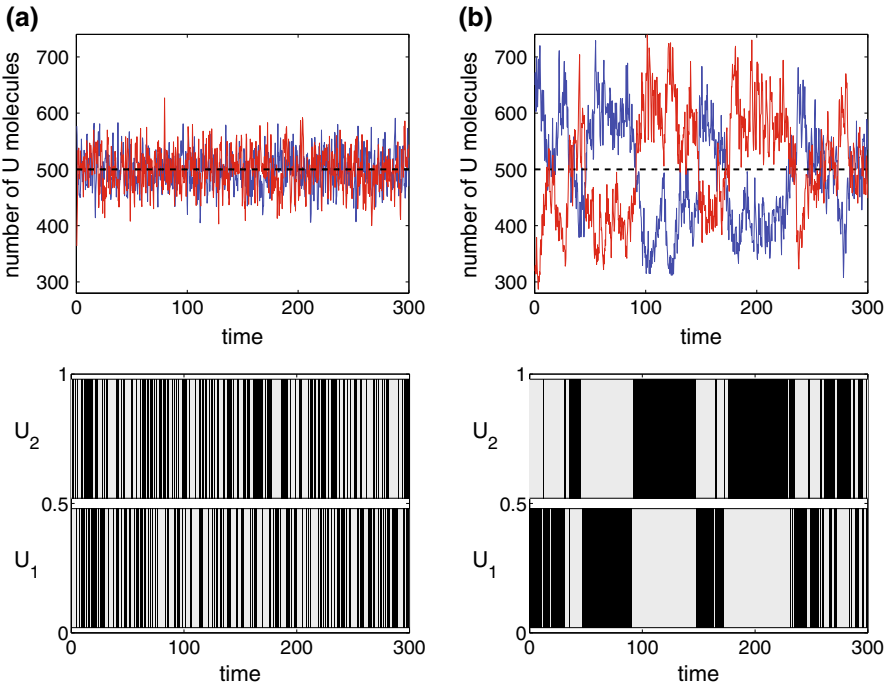

Fig. 7 Time evolution of U_1 (*blue line*) and U_2 (*red line*) for $K_u = K_v = 2$ is shown in *top panels* for **a** $D_u = 0.1$, $D_v = 0.4$ and **b** $D_u = 0.1$, $D_v = 10$. The corresponding time-dependent pattern is shown in *bottom panels* (Color figure online)

Thus, patterns are possible for some values of L provided that

$$\frac{D_v}{D_u} > 20 + 8\sqrt{6} \approx 39.6. \tag{46}$$

This condition is also the condition for the Turing patterns to emerge for the original system of mean-field PDEs (8)–(9).

4 Comparison of Compartment-Based Models for $K_u > 2$

The condition (27) for the generalized compartment-based model is only a necessary condition for the condition (43) for the classical case as we showed in Fig. 6. The bistability condition difference suggests that, if we use different discretizations for U and V, the stability of the homogeneous system may change. In this section, we compare the generalized and classical compartment-based models for $K_u > 2$. In Fig. 8, we use $D_u = 5 \times 10^{-4}$ and $D_v = 20 D_u$. In this case, the condition for (deterministic) Turing patterns (46) is not satisfied. The classical compartment-based model also does not show Turing patterns as it is demonstrated in Fig. 8a (with $K_u = K_v = 64$ compartments) and Fig. 8b (with $K_u = K_v = 8$ compartments). In both cases, no

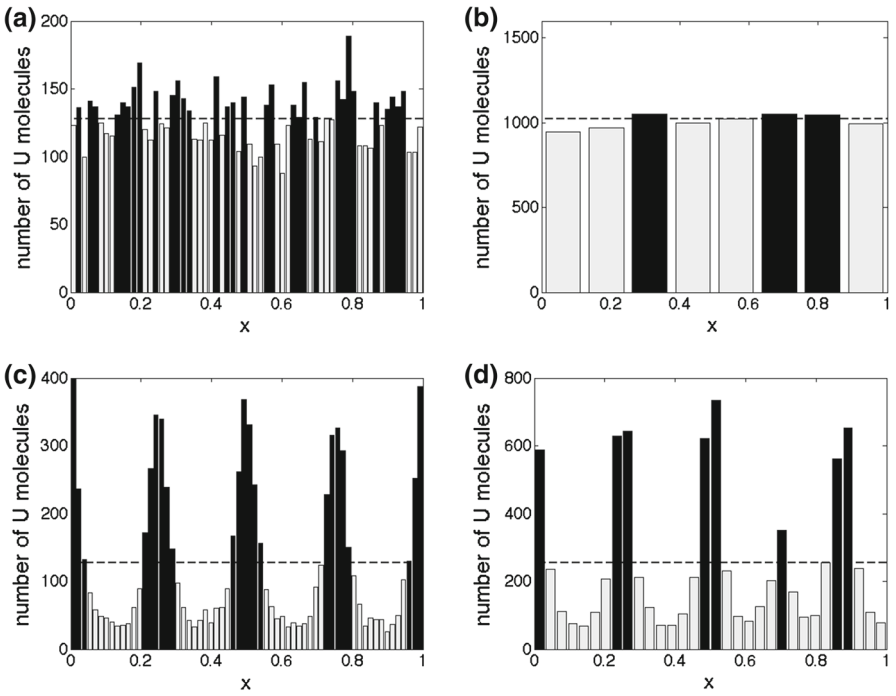

Fig. 8 Spatial distribution of U at time $T = 100$ for $D_v = 20D_u$, $\omega = 4096$ and $D_u = 5 \times 10^{-4}$ with **a** $K_u = K_v = 64$; **b** $K_u = K_v = 8$; **c** $K_u = 64$ and $K_v = 8$; **d** $K_u = 32$ and $K_v = 8$. There is no Turing pattern in the *top panels* (classical compartment-based model). Turing patterns appear in the *bottom panels* (generalized compartment-based model)

spatial Turing pattern is observed except noise from stochastic effects. However, if the generalized compartment-based model is used, then the Turing pattern may appear. In Fig. 8c, a result for the generalized compartment-based model with $K_u = 64$ and $K_v = 8$ is presented. There is a clear Turing pattern. In Fig. 8c, we have $\gamma = 8$. We also tested cases when $\gamma = 2$ and $\gamma = 4$ and obtained Turing patterns. The case $\gamma = 4$ is plotted in Fig. 8d.

In Fig. 9, we demonstrate that both discretizations strategies clearly show Turing patterns when we increase the ratio of diffusion constants to $D_v/D_u = 80$. In this case, the condition for (deterministic) Turing patterns (46) is satisfied. Finally, we present results for $D_v = 40D_u$ in Fig. 10. In the deterministic PDE system, when $D_v = 40D_u$, Turing pattern should still appear. But in the classical compartment-based model, it is hard to claim that there is a visible Turing pattern (see Figs. 10a, c). Considering the generalized compartment-based model, Turing patterns can be clearly observed (see Fig. 10b, d).

5 Discussion

We have shown that two choices of compartments illustrated in Fig. 2 can give different parameter regions for stochastic Turing patterns. An obvious question is which one

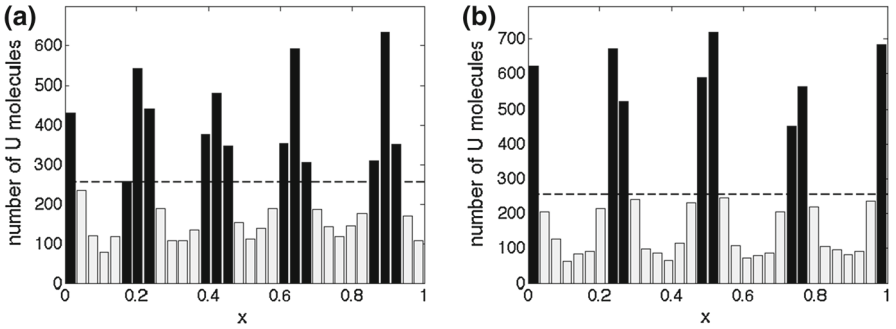

Fig. 9 Spatial distribution of U at time $T = 100$ for $D_v = 80D_u$. Both discretization strategies clearly show Turing patterns. We use $\omega = 4096$, $D_u = 5 \times 10^{-4}$ with **a** $K_u = K_v = 32$; **b** $K_u = 32$ and $K_v = 8$

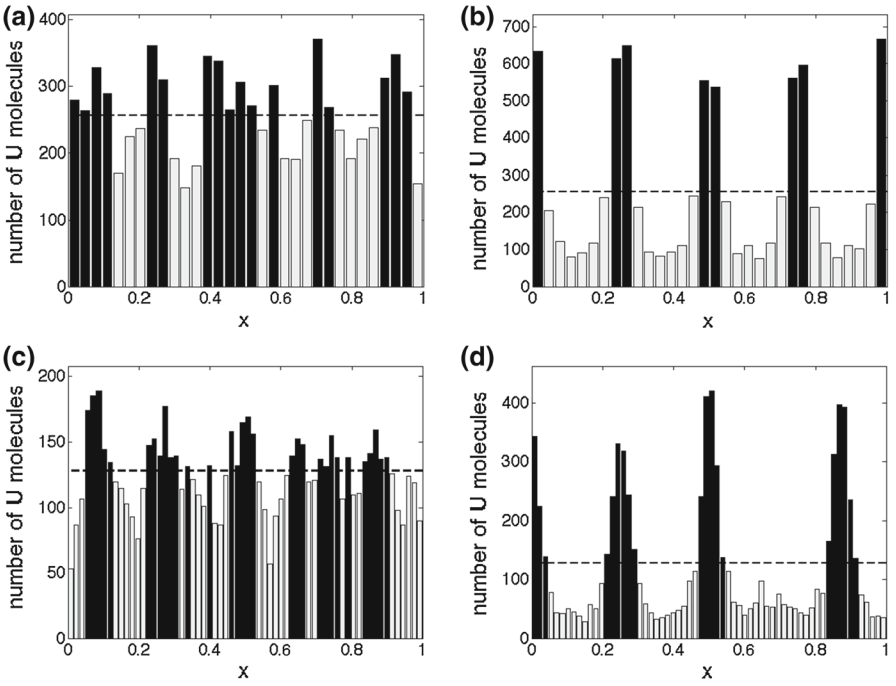

Fig. 10 Spatial distribution of U at time $T = 100$ for $D_v = 40D_u$. The generalized compartment-based model clearly shows Turing patterns, while it is difficult to see whether Turing patterns appear in the classical compartment-based model. We use $\omega = 4096$, $D_u = 5 \times 10^{-4}$ with **a** $K_u = K_v = 32$; **b** $K_u = 32$ and $K_v = 8$; **c** $K_u = K_v = 64$; **d** $K_u = 64$ and $K_v = 8$

is correct. One possibility to address this question is to consider a more detailed molecular-based approach which would be written in the form of Brownian dynamics (Erban and Chapman 2009). We are currently working on such a simulation, and we will report our findings in a future publication.

Although our results might look like a warning against the use of compartment-based methods for patterns based on the Turing mechanism, there are very good

reasons to use the compartment-based model in other situations (Engblom et al. 2009; Isaacson and Peskin 2006). Compartment-based models are often less computationally intensive than detailed Brownian dynamics simulations (Flegg et al. 2012; Hellander et al. 2012). They can be used for developing efficient multiscale methods where parts of the domain are simulated using the detailed Brownian dynamics while the rest of the domain is simulated using compartments (Erban et al. 2014; Flegg et al. 2013). They can also be used to bridge Brownian dynamics simulations with macroscopic PDEs (Ferm et al. 2010), because direct multiscale methods for coupling Brownian dynamics with PDEs are challenging to implement (Franz et al. 2013).

We have shown in Fig. 9 that the resulting patterns are comparable when the ratio of diffusion constants is sufficiently large. In this case, the generalized compartment-based model could also be used to construct computational approaches to speed-up simulations of the standard compartment-based model, because it does not simulate all diffusion events for chemical species with large diffusion constants (Li and Cao 2012, 2014). This multigrid discretization strategy has been recently applied in the modeling and simulation of a spatiotemporal model of PopZ localization in *Caulobacter crescentus* (Subramanian et al. 2014). In this model, the PopZ localization demonstrates a clear Turing pattern that can be modeled by a variation of the Schnakenberg model (6). The ratio of diffusion constants is sufficiently large, because PopZ monomers (variable V) diffuse (by three orders of magnitude) faster than PopZ polymers (variable U). Thus, the multigrid discretization strategy can be safely applied, and there is a significant speedup in numerical simulation (Subramanian et al. 2014).

Acknowledgments The research leading to these results has received funding from the European Research Council under the *European Community's* Seventh Framework Programme *(FP7/2007-2013)* / ERC *Grant Agreement* No. 239870. This publication was based on work supported in part by Award No. KUK-C1-013-04, made by King Abdullah University of Science and Technology (KAUST). Radek Erban would also like to thank the Royal Society for a University Research Fellowship; Brasenose College, University of Oxford, for a Nicholas Kurti Junior Fellowship; and the Leverhulme Trust for a Philip Leverhulme Prize. Yang Cao's work was supported by the National Science Foundation under awards DMS-1225160 and CCF-0953590, and the National Institutes of Health under award GM078989.

References

Asslani M, Di Patti F, Fanelli D (2012) Stochastic Turing patterns on a network. Phys Rev E 86:046105

Barrass I, Crampin E, Maini P (2006) Mode transitions in a model reaction-diffusion system driven by domain growth and noise. Bull Math Biol 68:981–995

Biancalani T, Fanelli D, Di Patti F (2010) Stochastic Turing patterns in a Brusselator model. Phys Rev E 81:046215

Biancalani T, Galla T, McKane A (2011) Stochastic waves in a Brusselator model with nonlocal interaction. Phys Rev E 84:026201

Black A, McKane A (2012) Stochastic formulations of ecological models and their applications. Trends Ecol Evolut 27(6):337–345

Butler T, Goldenfeld N (2011) Fluctuation-driven Turing patterns. Phys Rev E 84:011112

Cao Y, Li H, Petzold L (2004) Efficient formulation of the stochastic simulation algorithm for chemically reacting systems. J Chem Phys 121(9):4059–4067

Crampin E, Gaffney E, Maini P (1999) Reaction and diffusion on growing domains: scenarios for robust pattern formation. Bull Math Biol 61:1093–1120

Engblom S, Ferm L, Hellander A, Lötstedt P (2009) Simulation of stochastic reaction-diffusion processes on unstructured meshes. SIAM J Sci Comput 31:1774–1797

Erban R, Chapman SJ (2007) Reactive boundary conditions for stochastic simulations of reaction-diffusion processes. Phys Biol 4(1):16–28
Erban R, Chapman SJ (2009) Stochastic modelling of reaction-diffusion processes: algorithms for bimolecular reactions. Phys Biol 6(4):046001
Erban R, Chapman SJ, Maini P (2007) A practical guide to stochastic simulations of reaction-diffusion processes. 35 pp. http://arxiv.org/abs/0704.1908
Erban R, Flegg M, Papoian G (2014) Multiscale stochastic reaction-diffusion modelling: application to actin dynamics in filopodia. Bull Math Biol 76(4):799–818
Fange D, Elf J (2006) Noise-induced Min phenotypes in *E. coli*. PLoS Computat Biol 2(6):637–648
Ferm L, Hellander A, Lötstedt P (2010) An adaptive algorithm for simulation of stochastic reaction-diffusion processes. J Comput Phys 229:343–360
Flegg M, Chapman J, Erban R (2012) The two-regime method for optimizing stochastic reaction-diffusion simulations. J R Soc Interface 9(70):859–868
Flegg M, Rüdiger S, Erban R (2013) Diffusive spatio-temporal noise in a first-passage time model for intracellular calcium release. J Chem Phys 138:154103
Franz B, Flegg M, Chapman J, Erban R (2013) Multiscale reaction-diffusion algorithms: PDE-assisted Brownian dynamics. SIAM J Appl Math 73(3):1224–1247
Fu Z, Xu X, Wang H, Quoyang Q (2008) Stochastic simulation of Turing patterns. Chin Phys Lett 25(4):1220–1223
Gibson M, Bruck J (2000) Efficient exact stochastic simulation of chemical systems with many species and many channels. J Phys Chem A 104:1876–1889
Gillespie D (1977) Exact stochastic simulation of coupled chemical reactions. J Phys Chem 81(25):2340–2361
Hattne J, Fange D, Elf J (2005) Stochastic reaction-diffusion simulation with MesoRD. Bioinformatics 21(12):2923–2924
Hellander A, Hellander S, Lötstedt P (2012) Coupled mesoscopic and microscopic simulation of stochastic reaction-diffusion processes in mixed dimensions. Multiscale Modeling Simul 10(2):585–611
Hellander S, Hellander A, Petzold L (2012) Reaction-diffusion master equation in the microscopic limit. Phys Rev E 85:042901
Hori Y, Hara S (2012) Noise-induced spatial pattern formation in stochastic reaction-diffusion systems. In: Proceedings of 51st IEEE Conference on Decision and Control, pp 1053–1058
Hu J, Kang H, Othmer H (2014) Stochastic analysis of reaction-diffusion processes. Bull Math Biol 76(4):854–894
Isaacson S (2009) The reaction-diffusion master equation as an asymptotic approximation of diffusion to a small target. SIAM J Appl Math 70(1):77–111
Isaacson S, Peskin C (2006) Incorporating diffusion in complex geometries into stochastic chemical kinetics simulations. SIAM J Sci Comput 28(1):47–74
Kang H, Zheng L, Othmer H (2012) A new method for choosing the computational cell in stochastic reaction-diffusion systems. J Math Biol 65(6–7):1017–1099
Kepper P, Castets V, Dulos E, Boissonade J (1991) Turing-type chemical patterns in the chlorite-iodide-malonic acid reaction. Phys D 49:161–169
Li F, Cao Y (2012) Multiscale discretization for reaction diffusion systems. In: Proceedings of the 2012 International Conference on Bioinformatics and Computational Biology (Editors: Hamid R. Arabnia, Quoc-Nam Tran Associate Editors: Andy Marsh, Ashu M. G. Solo), Las Vegas, Nevada, USA, pp 305–311
Li F, Cao Y (2014) Optimal discretization size and multigrid discretization method for 1D multiscale reaction diffusion systems (submitted)
Maini P, Woolley T, Baker R, Gaffney E, Seirin Lee S (2012) Turing's model for biological pattern formation and the robustness problem. Interface Focus 2:487–496
McKane A, Biancalani T, Rogers (2014) Stochastic pattern formation and spontaneous polarization: the linear noise approximation and beyond. Bull Math Biol 76(4):859–921
Murray J (2002) Mathematical biology. Springer, Berlin
Qiao L, Erban R, Kelley C, Kevrekidis I (2006) Spatially distributed stochastic systems: equation-free and equation-assisted preconditioned computation. J Chem Phys 125:204108
Quyang Q, Swinney H (1991) Transition from a uniform state to hexagonal and striped Turing patterns. Nature 352:610–612
Satnoianu R, Menzinger M, Maini P (2000) Turing instabilities in general systems. J Math Biol 41:493–512

Schnakenberg J (1979) Simple chemical reaction systems with limit cycle behaviour. J Theor Biol 81:389–400

Scott M, Poulin F, Tang H (2011) Approximating intrinsic noise in continuous multispecies models. Proc R Soc A 467:718–737

Sick S, Reinker S, Timmer J, Schlake T (2006) WNT and DKK determine hair follicle spacing through a reaction-diffusion mechanism. Science 314:1447–1450

Subramanian K, Li F, Paul MR, Cao Y, Tyson JJ (2014) Spatiotemporal model of PopZ localization in *Caulobacter crescentus* (in preparation)

Turing A (1952) The chemical basis of morphogenesis. Philos Trans R Soc Lond 237:37–72

Twomey A (2007) On the stochastic modelling of reaction-diffusion processes. M.Sc. Thesis, University of Oxford, United Kingdom, September 2007.

Vigelius M, Meyer B (2012) Stochastic simulations of pattern formation in excitable media. PLoS One 7(8):e45208

Woolley T, Baker R, Gaffney E, Maini P (2011a) Power spectra methods for a stochastic description of diffusion on deterministically growing domains. Phys Rev E 84:021915

Woolley T, Baker R, Gaffney E, Maini P (2011b) Stochastic reaction and diffusion on growing domains: understanding the breakdown of robust pattern formation. Phys Rev E 84:046216

Woolley T, Baker R, Gaffney E, Maini P, Seirin-Lee S (2012) Effects of intrinsic stochasticity on delayed reaction-diffusion patterning systems. Phys Rev E 85:051914